Published in final edited form as:
Nat Med. 2006 April ; 12(4): 433–440. doi:10.1038/nm1390.

Newly expressed SUR1-regulated $NC_{Ca\text{-}ATP}$ channel mediates cerebral edema after ischemic stroke

J Marc Simard[1,2,3], **Mingkui Chen**[1], **Kirill V Tarasov**[1], **Sergei Bhatta**[1], **Svetlana Ivanova**[1], **Ludmila Melnitchenko**[1], **Natalya Tsymbalyuk**[1], **G Alexander West**[4], and **Volodymyr Gerzanich**[1]

[1]Department of Neurosurgery, School of Medicine, University of Maryland at Baltimore, 22 South Greene Street, Suite 12SD, Baltimore, Maryland 21201−1595, USA.

[2]Department of Pathology, School of Medicine, University of Maryland at Baltimore, 22 South Greene Street, Suite 12SD, Baltimore, Maryland 21201−1595, USA.

[3]Department of Physiology, School of Medicine, University of Maryland at Baltimore, 22 South Greene Street, Suite 12SD, Baltimore, Maryland 21201−1595, USA.

[4]Department of Neurological Surgery, Oregon Health & Science University, 3181 SW Sam Jackson Park Road, Portland, Oregon 97239−3098, USA.

Abstract

Pathological conditions in the central nervous system, including stroke and trauma, are often exacerbated by cerebral edema. We recently identified a nonselective cation channel, the $NC_{Ca\text{-}ATP}$ channel, in ischemic astrocytes that is regulated by sulfonylurea receptor 1 (SUR1), is opened by depletion of ATP and, when opened, causes cytotoxic edema. Here, we evaluated involvement of this channel in rodent models of stroke. SUR1 protein and mRNA were newly expressed in ischemic neurons, astrocytes and capillaries. Upregulation of SUR1 was linked to activation of the transcription factor Sp1 and was associated with expression of functional $NC_{Ca\text{-}ATP}$ but not K_{ATP} channels. Block of SUR1 with low-dose glibenclamide reduced cerebral edema, infarct volume and mortality by 50%, with the reduction in infarct volume being associated with cortical sparing. Our findings indicate that the $NC_{Ca\text{-}ATP}$ channel is crucially involved in development of cerebral edema, and that targeting SUR1 may provide a new therapeutic approach to stroke.

Edema complicates many conditions that affect the central nervous system (CNS), including stroke and trauma. Edema worsens neurological function and can threaten life. Swelling resulting from malignant cerebral edema after a large middle cerebral artery (MCA) stroke is responsible for the high mortality of 60−80% of the patients[1]. Molecular mechanisms of cerebral edema are poorly understood, and available treatments are nonspecific and only moderately effective[1].

SUR1 is a regulatory subunit that associates with Kir6.*x* pore-forming subunits to form heterooctameric K_{ATP} channels[2]. SUR1 confers sensitivity to sulfonylurea inhibitors such as glibenclamide and to channel activators such as diazoxide. Apart from involvement with

Correspondence should be addressed to J.M.S. (msimard@surgery1.umaryland.edu)..

COMPETING INTERESTS STATEMENT
The authors declare competing financial interests (see the *Nature Medicine* website for details).

K_{ATP} channels, SUR1 also regulates activity of a nonselective cation channel, the $NC_{Ca\text{-}ATP}$ channel[3]. First identified in freshly isolated (but not cultured) reactive astrocytes, this channel conducts monovalent cations, requires nanomolar concentrations of intracellular Ca^{2+} for opening, and is activated by depletion of intracellular ATP[4]. Opening of $NC_{Ca\text{-}ATP}$ channels causes complete depolarization and cell blebbing, characteristic of cytotoxic edema. Depolarization and blebbing induced by depletion of ATP are prevented by glibenclamide, and are reproduced without depletion of ATP by diazoxide, consistent with a crucial role for $NC_{Ca\text{-}ATP}$ channels in cytotoxic edema[3].

Because the $NC_{Ca\text{-}ATP}$ channel was first discovered in hypoxic gliotic tissues, we postulated that other causes of hypoxia, including arterial occlusion, might also be associated with channel expression. We thus studied rodent models of stroke (permanent focal cerebral ischemia) after MCA occlusion (MCAO). For most of our experiments, we used a model of massive MCA infarction associated with malignant cerebral edema (MCE) and high mortality. Alternatively, to study effects on infarct volume, we used a thromboembolic model associated with nonlethal infarctions. Here, we report that expression of $NC_{Ca\text{-}ATP}$ channels is upregulated after MCAO, and that block by low-dose glibenclamide results in major improvements in stroke outcome.

RESULTS

Upregulation of SUR1 in MCE model

We used immunohistochemical analysis and immunoblots to determine expression of SUR1 in three regions after ischemia: the uninvolved hemisphere, the peri-infarct region, and the core of the infarct, with the core identified by absence of perfusion (Fig. 1a), absence of 2,3,5-triphenyltetrazolium chloride (TTC) staining[5] (Fig. 1b) and absence of glial fibrillary acidic protein (GFAP) immunolabeling[6] (data not shown).

In the core, levels of SUR1 increased significantly above background levels 2−3 h after MCAO (Fig. 1c–g). Unlike contralateral tissues, virtually every $NeuN^+$ cell (Fig. 1d) and capillary in the core was positive for SUR1, with labeling also evident in some $NeuN^-$ cells. Levels of SUR1 remained elevated at 6 h, but declined by 8 h (Fig. 1g), coinciding with the appearance of necrosis. At all times, SUR1 in the core far exceeded levels in contralateral regions[7,8] (Fig. 1g).

In TTC^+ peri-infarct regions, levels of SUR1 increased later than in the core, but the increase was sustained (Fig. 1g). By 8−16 h after MCAO, SUR1 sharply demarcated core and peri-infarct regions (Fig. 1c), and was evident in $NeuN^+$ neurons, $GFAP^+$ astrocytes (Fig. 1e) and von Willebrand $factor^+$ capillary endothelial cells (Fig. 1f).

Immunohistochemical changes in expression of SUR1 at 8 h (Fig. 1g) were confirmed by immunoblots at 8 h (Fig. 2a,b). Also, immunoblots of TTC^+ peri-infarct regions, where necrosis could not confound antibody binding, showed that levels of SUR1 increased progressively over 8 h to approximately three times higher than control levels (Fig. 2a,b). We confirmed the specificity of the antibody used for immunohistochemistry and immunoblots in separate experiments (Fig. 2b).

The ischemia-induced increase in SUR1 was corroborated by measurements of *Abcc8* mRNA (encoding SUR1), which increased two- to threefold in the core at 3 h (Fig. 2c). *In situ* hybridization showed that SUR1 transcripts were present in neurons and capillaries in the core but not in control tissues (Fig. 2d–g). Thus, cerebral ischemia resulted in substantial transcriptional upregulation of SUR1.

Sp1 and Sp3 transcription factors

The promoter region of *Abcc8* contains consensus sequences for binding Sp1, and Sp1 drives expression of SUR1 in a concentration-dependent manner[9,10]. In the core of the infarct, nuclear labeling for Sp1 was evident at 1 h and was more prominent 3 h after MCAO, especially in large neuron-like cells (Fig. 3a,b). Double immunolabeling showed that many $Sp1^+$ cells also labeled for SUR1 (Fig. 3c). In peri-infarct areas, nuclear localization of Sp1 was evident in capillaries and in other cells at 3−6 h (Fig. 3d,e). Immunoblots of nuclear extracts showed a three- to fourfold increase in nuclear Sp1 in the core, compared to control (Fig. 3f). Expression of Sp3, which may ultimately determine transcriptional activity of Sp1 by virtue of its inhibition of Sp1 binding, was unchanged (Fig. 3f).

Sp1 is a key driver of SUR1 expression *in vitro*[9,10], but this association has not been validated for CNS cells *in vivo*. Chromatin immunoprecipitation of DNA extracted from the core 2 h after MCAO using Sp1-specific antibody showed prominent PCR products for the Sp1 binding region of the *Abcc8* promoter, but not for the promoter region of *Crp*, which encodes C-reactive protein (Fig. 3g) and which has no consensus binding sites for Sp1. Thus, transcriptional upregulation of SUR1 in cerebral ischemia could be ascribed, at least in part, to activation of Sp1.

$NC_{Ca\text{-}ATP}$ channel in neurons after MCAO

Although SUR1 was upregulated in cerebral ischemia, the pore-forming subunits of K_{ATP} channels, Kir6.1 or Kir6.2, were not (Fig. 2b). Apart from its involvement in K_{ATP} channels, SUR1 also forms the regulatory subunit of $NC_{Ca\text{-}ATP}$ channels[3]. As the pore-forming subunit of the $NC_{Ca\text{-}ATP}$ channel has not been cloned, we used its biophysical properties for identification. We studied inside-out patches of large neuron-like cells isolated from the core 2 h and 6 h after MCAO (Fig. 4a–d). Using Cs^+ as the charge carrier to block K^+ channels, including K_{ATP}, we found that neurons from the core expressed channels that: (i) conducted Cs^+; (ii) were strongly inhibited by ATP on the cytoplasmic side; (iii) required Ca^{2+} on the cytoplasmic side for activity (Fig. 4b); and (iv) were blocked by glibenclamide (Fig. 4d). Each of these four characteristic findings[3,4] was replicated in three to six patches from 15 rats with MCAO. Patches from eight neurons dissociated from contralateral regions and studied in the same manner, including Cs^+ as the charge carrier, showed no channel activity. In neurons from the core, when we used K^+ as the charge carrier, we observed a glibenclamide-sensitive, Ca^{2+}-dependent single-channel conductance of 34 pS (Fig. 4c), consistent with the $NC_{Ca\text{-}ATP}$ channel[4] but not K_{ATP} channels[2]. The ability to conduct Cs^+, the requirement for Ca^{2+} and a single-channel conductance of 34 pS with K^+ unambiguously distinguish the $NC_{Ca\text{-}ATP}$ channel from K_{ATP} channels. Thus, upregulation of SUR1 in cerebral ischemia was associated with expression of $NC_{Ca\text{-}ATP}$ but not K_{ATP} channels.

Glibenclamide is a potent blocker of $NC_{Ca\text{-}ATP}$ channels (50% effective concentration (EC_{50}) = 48 nM at pH 7.4, 22 °C)[3]. In neurons from the core, 50 nM glibenclamide (pH 7.4) reduced the open probability of $NC_{Ca\text{-}ATP}$ channels to 56.1 ± 6.5% of baseline values (Fig. 4d). It is the un-ionized form of the weak acid, glibenclamide (pK_a 6.3), however, that is responsible for channel block[11,12], and at pH 7.4, only 7% is un-ionized. We reasoned that the apparent potency of glibenclamide would increase at the acidic pH found in ischemic brain[13]. In the same neurons from the core, reducing the pH to 6.8 decreased the open probability with 50 nM glibenclamide to 12.0 ± 4.4% of baseline values (Fig. 4d), consistent with block by the un-ionized form.

Glibenclamide is cytoprotective

Opening of $NC_{Ca\text{-}ATP}$ channels after sodium azide–induced depletion of ATP results in cytotoxic edema (oncotic cell blebbing)[3,4], a precursor of oncotic cell death. We postulated

that block of this channel by glibenclamide would protect cells from death. We tested this using astrocytes freshly isolated from the ischemic inner zone of gliotic capsules, where $NC_{Ca\text{-}ATP}$ channels are expressed[3,4]. Exposure of the cells to sodium azide resulted in a high incidence of oncotic death, as indicated by nuclear labeling with propidium iodide (Fig. 4e,g). Apoptotic death, as measured by annexin V labeling, was not prominent (Fig. 4f,g). Pretreatment with glibenclamide before exposure to sodium azide resulted in a significant reduction in cell death ($P < 0.01$; Fig. 4e,g), showing cytoprotection by glibenclamide in the context of depletion of ATP after ischemia.

Glibenclamide treatment in MCE model

To determine the role of $NC_{Ca\text{-}ATP}$ channels in cerebral ischemia, we studied the effects of glibenclamide, the highly selective inhibitor of SUR1 (ref. [14-16]). We used constant infusion of a low dose of drug to achieve sustained occupancy of only high-affinity receptors. In a large group of male and female rats with MCAO (MCE model), treatment with glibenclamide resulted in a marked reduction in mortality compared to treatment with saline, from 65% to 24% ($P < 0.002$; Fig. 5a). Delayed deaths were not observed with glibenclamide, indicating that the effect was durable.

As glibenclamide prevents cytotoxic edema[3,4], we postulated that the beneficial effect on mortality might be the result of a reduction in cerebral edema. We studied the effect of glibenclamide on cerebral edema 8 h after MCAO, a time that preceded death of any rat in the mortality study. In the first of two experiments, we compared water content in the involved and uninvolved hemispheres. For the control hemisphere, water was 77.9 ± 0.2% of tissue wet weight. For the involved hemisphere, water increased by 3.4%, to 81.3 ± 0.5% for the saline-treated group, whereas it increased by only 2.0%, to 79.9 ± 0.3%, for the glibenclamide-treated group ($P < 0.05$), consistent with an important role for SUR1-regulated $NC_{Ca\text{-}ATP}$ channels in formation of edema.

After stroke, a cerebral hemisphere includes normal, infarcted and ischemic peri-infarct tissues, each of which contains different amounts of water. To characterize the location of edema at 8 h, we measured water content after dividing tissues into viable TTC^+ and nonviable TTC^- portions. Water in the uninvolved hemisphere was 78.0 ± 0.1% (Fig. 5b), similar to the previous value of 77.9 ± 0.2%, indicating that TTC processing had not altered water content. For the involved hemisphere, water in TTC^+ tissues increased by 5.4% or 5.9%, to 83.4 ± 1.1% or 83.6 ± 0.9%, for groups treated with either saline alone or with vehicle, respectively, whereas it increased by only 2.3%, to 80.5 ± 0.3% ($P < 0.05$), for the glibenclamide-treated group (Fig. 5b). In contrast, values for water in TTC^- tissues, 78.7 ± 1.0%, 78.4 ± 0.8% and 78.6 ± 0.4% with saline, vehicle and glibenclamide, respectively, were only slightly higher ($P = 0.97$) than values for the uninvolved hemisphere (78.0%), reflecting a need for blood flow to form edema (Fig. 5b)[1]. Together, these data indicate that excess water originated predominantly from peri-infarct regions, and that glibenclamide was highly effective in reducing it.

The previous data indicate that protective effects of glibenclamide could not be attributed to dimethylsulfoxide in the vehicle. As additional controls, we considered potential effects of glibenclamide on serum glucose and on blood pressure. When measured in rats from the edema studies, serum glucose at 8 h was decreased by glibenclamide (122 ± 4 versus 93 ± 3 mg/dl; $P < 0.05$; 11 rats/group). The reduction was significant, confirming that serum levels of glibenclamide were sufficient to affect pancreatic SUR1, but such levels of glucose are not associated with altered outcome in ischemia[17,18]. Systolic blood pressure measured at 8 h was not affected by glibenclamide (120 ± 7 versus 109 ± 6 mmHg; $P = 0.26$; 11 rats/group).

Glibenclamide treatment in thromboembolic model

Given the marked effects on mortality and edema, we sought to determine the effect of glibenclamide on infarct volume. This was not feasible with the MCE model because of high early mortality. We therefore utilized a nonlethal thromboembolic model to assess infarct volume at 2 and 7 d after MCAO. At 2 d, glibenclamide treatment resulted in a highly significant reduction in infarct volume, compared to controls treated with saline (35.5 ± 4.4% versus 16.7 ± 2.2%; $P < 0.01$; Fig. 5c–e). We made a similar observation at 7 d (15.2 ± 1.2%; $P < 0.01$), again indicating that effects of treatment were durable.

All rats, regardless of treatment group, suffered infarctions involving the basal ganglia, which are supplied by terminal arterioles. Reduced infarct volumes in the glibenclamide-treated groups, however, were often associated with marked sparing of the cerebral cortex (Fig. 5c,d), a phenomenon previously reported with decompressive craniectomy[19].

We hypothesized that cortical sparing with glibenclamide might reflect improved leptomeningeal collateral blood flow, which could result from reduced cerebral edema, but not from direct vasodilation, because normally glibenclamide is vasoconstrictive as a result of block of K_{ATP} channels[20,21]. Using the same thromboembolic model, we obtained measurements of relative cerebral blood flow for somatosensory cortex supplied by the MCA. Laser Doppler flowmetry showed values in the involved hemisphere that were significantly reduced 1 h after MCAO in both saline- and glibenclamide-treated groups (Fig. 5f). Flow recovered completely by 48 h, however, in glibenclamide- but not saline-treated rats (Fig. 5f), consistent with the cortical sparing observed.

Tissue distribution of glibenclamide in MCE model

Low-dose glibenclamide was unexpectedly effective in reducing mortality, cerebral edema and infarct volume, yet had only a small effect on serum glucose. We thus sought to confirm that glibenclamide was reaching targeted areas of cerebral ischemia.

We used the fluorescent derivative, BODIPY-glibenclamide, to examine drug distribution 8 h after MCAO. Administration of the labeled compound at the same rate and molar concentration as the parent compound (cumulative dose, 1.2 nmol in 8 h) yielded no labeling in the uninvolved hemisphere (Fig. 6a,b), consistent with exclusion by normal blood-brain barrier, and none in the core of the infarct (data not shown), consistent with absence of perfusion. There was weak labeling in pancreatic islets of Langerhans, but prominent labeling in peri-infarct regions (Fig. 6a), with labeling of large neuron-like cells and microvessels (Fig. 6a), including capillaries (Fig. 6c), that showed expression of SUR1 (Fig. 6d). Labeling in peri-infarct tissues reflected not only an increase in SUR1 glibenclamide-binding sites, which show femtomolar binding affinity for glibenclamide[22,23], but also indicated that normal permeability barriers no longer excluded the drug. Selective distribution of drug to peri-infarct tissues may have been facilitated by breakdown of the blood-brain barrier, but was undoubtedly driven by an increase in lipid solubility of the weak acid, glibenclamide, as a result of the low pH of ischemic peri-infarct tissues[13].

DISCUSSION

Here, we show that SUR1 is transcriptionally upregulated in focal cerebral ischemia, initially in the core, and later in peri-infarct regions, with involvement of neurons, astrocytes and capillary endothelial cells. Ischemia-induced upregulation of SUR1 was attributable, at least in part, to activation of the transcription factor Sp1. Sp1 has previously been shown to be a crucial driver of SUR1 expression[9,10], and activation of Sp1 has previously been associated

with ischemia-hypoxia[24,25]; but our data show Sp1 activation in cerebral ischemia and link this with expression of SUR1.

SUR1 forms the regulatory subunit of both K_{ATP} and $NC_{Ca\text{-}ATP}$ channels. Based on immunoblots for Kir6.1 or Kir6.2 and on electrophysiological experiments, we found that K_{ATP} channels were not upregulated, whereas $NC_{Ca\text{-}ATP}$ channels were. The $NC_{Ca\text{-}ATP}$ channel was previously characterized in astrocytes[3,4], and here we identified it in neurons after onset of ischemia. The key biophysical properties that distinguish $NC_{Ca\text{-}ATP}$ from K_{ATP} channels include: (i) nonselective monovalent cation conductivity, including for Cs^+, which is a blocker of K_{ATP} channels; (ii) a requirement for intracellular Ca^{2+}, which does not exist for K_{ATP} channels; and (iii) a single-channel conductance of 34 pS with K^+, which is 50% of that for K_{ATP} channels[2]. These three properties are probably attributable to the pore-forming subunits, as the SUR1 regulatory subunits of the two channels are functionally indistinguishable.

Cerebral edema is a complex pathophysiological process that causes brain swelling, neurological dysfunction and may ultimately lead to brain herniation and death[1,26]. Cerebral edema initially results from formation of ‘cytotoxic’ (cellular) edema, which is inextricably bound to cell death. Cytotoxic edema, which forms early in the core of the infarct, depletes the extracellular space of Na^+, creating a concentration gradient for Na^+ between infarct and peri-infarct regions. This gradient later drives passive transcapillary flux of Na^+ that is integral to formation of ‘ionic’ edema in peri-infarct regions[27]. In both cytotoxic and ionic edema, movements of Na^+ are accompanied by secondary movements of Cl^- and H_2O, driven by electrical and osmotic forces. The molecular entity, channel or otherwise, that allows passive movement of Na^+ down its electrochemical gradient has not been previously identified. We hypothesize that newly expressed $NC_{Ca\text{-}ATP}$ channels constitute this heretofore unidentified pathway for Na^+ flux required for formation of edema. Block of this channel by glibenclamide is highly effective in preventing Na^+ influx, cell depolarization and cell blebbing, all hallmarks of cytotoxic edema, in isolated cells *in vitro* that express the $NC_{Ca\text{-}ATP}$ channel[3,4]. Here, we show in the same cells that glibenclamide also protects from cell death, the ultimate consequence of cytotoxic edema. Moreover, we show that glibenclamide *in vivo* is highly effective in reducing accumulation of excess brain water, the hallmark of ionic edema, in peri-infarct tissues that express the $NC_{Ca\text{-}ATP}$ channel. It seems that, *in vivo*, early upregulation of $NC_{Ca\text{-}ATP}$ channels in neurons in the core is associated with formation of cytotoxic edema, whereas later upregulation of $NC_{Ca\text{-}ATP}$ channels in capillaries in peri-infarct regions is associated with formation of ionic edema.

Numerous neuroprotective strategies assessed over the last decade have failed in human trials, in part as a result of dose-limiting side effects. In contrast, glibenclamide has been used safely in humans for several decades for treatment of type 2 diabetes, with no untoward side effects except hypoglycemia. We found that constant infusion of low-dose glibenclamide caused only slight reduction of serum glucose, but was highly effective in reducing cerebral edema, infarct volume and mortality in rodent models of stroke. Three features combine to maximize beneficial effects while minimizing potential side effects of glibenclamide: (i) its molecular target resides within the lipid plasmalemmal membrane[11,12]; (ii) as a weak acid, its lipophilicity, which determines its ability to reach its target, increases in acidic medium; and (iii) targeted ischemic tissues are acidic[13]. Thus, the safety of glibenclamide, as borne out by decades of use in humans, and the efficacy of glibenclamide, as shown here, indicate that glibenclamide may be particularly attractive for translational use in human stroke.

The neuroprotection afforded by glibenclamide, which we observed at both the cellular and organ levels, predicts that glibenclamide would also improve functional neurological outcome in stroke. Moreover, the time required for transcriptional upregulation of $NC_{Ca\text{-}ATP}$ channels

after onset of ischemia predicts that glibenclamide would have a favorable therapeutic time window. Overall, our data indicate that molecular therapies directed at the SUR1-regulated $NC_{Ca\text{-}ATP}$ channel may provide new avenues of treatment for CNS injuries associated with ischemia.

METHODS

MCAO

Protocols were approved by the Institutional Animal Care and Use Committee of the University of Maryland. We fasted Wistar rats (275−350 g) overnight, anesthetized them (ketamine, 60 mg/kg; xylazine, 7.5 mg/kg, intraperitoneally) and maintained their body temperature at approximately 37 °C. For thromboembolic stroke, we embolized seven to eight allogeneic clots through the internal carotid artery[28]. For MCE, we embolized polyvinyl alcohol (PVA) microparticles (Target Therapeutics; 150−250 μm, 600 μg in 1.5 ml heparinized saline)[29], followed by standard permanent suture occlusion[30]. Blood gases (in mmHg) and glucose (in mg/dl) at time of MCAO: pO_2, 94 ± 5; pCO_2, 36 ± 5; pH, 7.33 ± 0.01; glucose, 142 ± 6 in controls; pO_2,93±3; pCO_2, 38 ± 2; pH, 7.34 ± 0.01; glucose 152 ± 7 in glibenclamide-treated rats. With the MCE model, rats showed delayed deterioration, often leading to death within 12 −24 h, with necropsies showing bland infarcts.

Drug delivery

Within 2−3 min after MCAO, we implanted miniosmotic pumps (Alzet 2002, 0.5 μl/hr; Durect Corporation) that delivered either PBS, vehicle (PBS plus DMSO), glibenclamide (Sigma) in vehicle, or BODIPY-FL-glyburide (Molecular Probes) in vehicle subcutaneously (no loading doses). We diluted 10 mM stock solutions of glibenclamide or BODIPY-FL-glyburide in DMSO in PBS to final concentrations of 300 μM in the pump. Infusion rates for glibenclamide and DMSO were 75 ng/h and 15 nl/h, respectively.

Edema

We measured edema using the wet/dry weight method with water content expressed as the percent of tissue wet weight as previously described[31].

Infarct volume

After TTC staining[5], we computed volume of TTC^- tissue in consecutive 2-mm thick slices as the percent hemisphere volume.

Laser Doppler flowmetry

Before MCAO, we drilled two 1.5-mm pits partway through the skull over MCA territory, with the depth adjusted to obtain a ratio of laser Doppler flowmetry readings of 1.0 between sides. We took five measurements (DRT4, Moor Instruments) at 1-min intervals. We used the means to calculate the ratio between sides.

Immunohistochemistry

We immunolabled cryosections[3] using primary antibodies directed against SUR1 (1:200; 1 h at 22 °C, 48 h at 4 °C), NeuN (1:100; MAB377; Chemicon), GFAP (1:500; C-9205; Sigma), von Willebrand factor (1:200; F3520; Sigma). We performed quantitative immunofluorescence as previously described[32].

Immunoblots

We prepared immunoblots as previously described[33]. We isolated nuclear proteins using CelLytic NuCLEAR EXTRACTION Kit (Sigma). Primary antibodies were directed against: acetyl-Histone H3 (Sigma), and SUR1, Kir6.1, Kir6.2, Sp1, Sp3 (all from Santa Cruz).

Specificity of SUR1 antibody

We confirmed specificity of SUR1-specific antibody (SC-5789; Santa Cruz), previously shown to block glibenclamide inhibition of $NC_{Ca\text{-}ATP}$ channels[3], using positive (pancreas, RIN-m5f cells, HepG2 cells, hippocampus) and negative (omission of primary antibody) controls. Immunoblots of normal and peri-infarct brain 8 h after MCAO showed labeling of one band (180 kDa) in the range of 116−290 kDa. Immunoblots of ischemic gliotic tissues showed labeling of one band at 180 kDa that was substantially reduced by *in vivo* knockdown of SUR1 expression (SUR1-KD). For SUR1-KD, we implanted rats with gelatin sponges in parietal lobes[3,4], and with miniosmotic pumps containing oligodeoxynucleotide (711 μg/ml delivered at 0.5 μl/h; 1,500 pmol/d), with the delivery catheter placed into the implant site. We infused controls with scrambled sequence oligodeoxynucleotide (5′-TGCCTGAGGCGTGGCTGT-3′); we infused SUR1-KD rats with SUR1-specific antisense oligodeoxynucleotide (5′-GGCCGAGTGGTTCTCGGT-3′). We immunoblotted gliotic tissues after 10−14 d; we performed experiments in triplicate. Patch clamp analysis showed that astrocytes from controls (scrambled sequence) expressed normal $NC_{Ca\text{-}ATP}$ channels, whereas astrocytes from SUR1-KD rats showed no $NC_{Ca\text{-}ATP}$ channels (J.M.S. & M.C., unpublished data).

Real-time-PCR

We reverse transcribed total RNA with random hexonucleotides (Applied Biosystems). We performed real-time PCR with an ABI PRISM 7300 (Applied Biosystems) using a TaqMan-based protocol. TaqMan probes and primers were selected with Primer Express 2.0 (Applied Biosystems) and synthesized by Applied Biosystems. Primer sequences were as follows: H1 histone, 5′-CGGACCACCCCAAGTATTCA-3′ (forward); 5′-GCCGGCACGGTTCTTCT-3′ (reverse); 5′-CATGATCGTGGCTGCTATCCAGGCA-3′ (TaqMan). For *Abcc8*, primers were as follows: 5′-GAGTCGGACTTCTCGCCCT-3′ (forward); 5′-CCTTGACAGTGGACCGAACC-3′ (reverse); 5′-TTCCACATCCTGGTCACACCGCTGT-3′ (TaqMan). We performed amplification of triplicate samples using a TaqMan amplification kit (Applied Biosystems) and quantification using a standard curve method.

In situ hybridization

We made digoxigenin-labeled probes (Roche) using SP6 or T7 RNA polymerase. We generated sense and antisense RNA digoxigenin-labeled probes from pGEM-T easy plasmids (Promega) with the *Abcc8* insert (613 bp) flanked by the following primers: 5′-AAGCACGTCAACGCCCT-3′ (forward); 5′-GAAGCTTTTCCGGCTTGTC-3′ (reverse). We labeled[34] sections in triplicate.

Chromatin immunoprecipitation

We performed chromatin immunoprecipitation[35] using the ChIP-IT kit (Active Motif) and Sp1-specific antibodies (07−645, Upstate). Detection of DNA after chomatin immunoprecipitation was performed by PCR using GC-Rich PCR system (Roche). Primers for the promoter region of *Abcc8* (91 bp) were as follows[10]: 5′-CTCGCCCCACAAGAGCATCT-3′, 5′-CTCGCAGCACCCTGGGCT-3′. Primers for the promoter region of *Crp* (121 bp) were as follows: 5′-TCTCAATATAGATAGGCAAAATGGA-3′, 5′-ACAGAGAAATCGATGTGGGTTA-3′ (provided by M. Volkova, US National Institutes of

Health, National Institute on Aging's Gerontology Research Center); this gene has no consensus binding sites for Sp1 (Gene2-Promoter). We used the following amplification protocol: 95 °C for 3 min; 35 cycles of 95 °C for 30 s, 61.5 °C for 30 s, 72 °C for 30 s.

Electrophysiology

For patch clamp studies[3,4], neurons were dissociated as described[36], except for vibratome slices 250 μm thick, and protease treatment lasted 15 min.

Cell death

We plated freshly isolated astrocytes[3,4] on four-well chamber slides (Lab-Tek, Nalge Nunc International) in physiological solution (10^4 cells/100 μl/well) supplemented with vehicle, 1 mM sodium azide or 1 μM glibenclamide followed 5 min later with 1 mM sodium azide. We assayed platelets 10 min after adding sodium azide, using propidium iodide and annexin V (Vybrant Apoptosis Assay Kit 2, Molecular Probes). We counted total number of cells, annexin V^+ and propidium $iodide^+$ cells in 20 fields under a ×20 objective lens.

Statistical analysis

Mortality data were compared by χ^2 analysis. Otherwise, we used Student *t*-test or ANOVA to determine statistical significance.

Accession codes

Entrez Gene: rat *Crp*, 25419.

ACKNOWLEDGMENTS

This work was supported by grants (to J.M.S.) from the National Institute of Neurological Disorders and Stroke (NS048260), National Heart, Lung, and Blood Institute (HL082517) and by a Merit Review Grant from the Veterans Affairs (Baltimore Veterans Affairs, Baltimore, Maryland, USA).

References

1. Ayata C, Ropper AH. Ischaemic brain oedema. J. Clin. Neurosci 2002;9:113–124. [PubMed: 11922696]
2. Seino S. ATP-sensitive potassium channels: a model of heteromultimeric potassium channel/receptor assemblies. Annu. Rev. Physiol 1999;61:337–362. [PubMed: 10099692]
3. Chen M, Dong Y, Simard JM. Functional coupling between sulfonylurea receptor type 1 and a nonselective cation channel in reactive astrocytes from adult rat brain. J. Neurosci 2003;23:8568–8577. [PubMed: 13679426]
4. Chen M, Simard JM. Cell swelling and a nonselective cation channel regulated by internal Ca^{2+} and ATP in native reactive astrocytes from adult rat brain. J. Neurosci 2001;21:6512–6521. [PubMed: 11517240]
5. Mathews KS, et al. Rapid quantification of ischaemic injury and cerebroprotection in brain slices using densitometric assessment of 2,3,5-triphenyltetrazolium chloride staining. J. Neurosci. Methods 2000;102:43–51. [PubMed: 11000410]
6. Chen H, Chopp M, Schultz L, Bodzin G, Garcia JH. Sequential neuronal and astrocytic changes after transient middle cerebral artery occlusion in the rat. J. Neurol. Sci 1993;118:109–116. [PubMed: 8229058]
7. Treherne JM, Ashford ML. The regional distribution of sulphonylurea binding sites in rat brain. Neuroscience 1991;40:523–531. [PubMed: 1902917]
8. Karschin C, Ecke C, Ashcroft FM, Karschin A. Overlapping distribution of K(ATP) channel-forming Kir6.2 subunit and the sulfonylurea receptor SUR1 in rodent brain. FEBS Lett 1997;401:59–64. [PubMed: 9003806]

9. Ashfield R, Ashcroft SJ. Cloning of the promoters for the beta-cell ATP-sensitive K-channel subunits Kir6.2 and SUR1. Diabetes 1998;47:1274–1280. [PubMed: 9703328]
10. Hernandez-Sanchez C, Ito Y, Ferrer J, Reitman M, LeRoith D. Characterization of the mouse sulfonylurea receptor 1 promoter and its regulation. J. Biol. Chem 1999;274:18261–18270. [PubMed: 10373428]
11. Findlay I. Effects of pH upon the inhibition by sulphonylurea drugs of ATP-sensitive K+ channels in cardiac muscle. J. Pharmacol. Exp. Ther 1992;262:71–79. [PubMed: 1625214]
12. Zunkler BJ, Trube G, Panten U. How do sulfonylureas approach their receptor in the B-cell plasma membrane? Naunyn Schmiedebergs Arch. Pharmacol 1989;340:328–332. [PubMed: 2682269]
13. Nedergaard M, Kraig RP, Tanabe J, Pulsinelli WA. Dynamics of interstitial and intracellular pH in evolving brain infarct. Am. J. Physiol 1991;260:R581–R588. [PubMed: 2001008]
14. Fujita A, Kurachi Y. Molecular aspects of ATP-sensitive K+ channels in the cardiovascular system and K+ channel openers. Pharmacol. Ther 2000;85:39–53. [PubMed: 10674713]
15. Gribble FM, Reimann F. Sulphonylurea action revisited: the post-cloning era. Diabetologia 2003;46:875–891. [PubMed: 12819907]
16. Proks P, Reimann F, Green N, Gribble F, Ashcroft F. Sulfonylurea stimulation of insulin secretion. Diabetes 2002;51(Suppl 3):S368–S376. [PubMed: 12475777]
17. Li PA, Shamloo M, Smith ML, Katsura K, Siesjo BK. The influence of plasma glucose concentrations on ischemic brain damage is a threshold function. Neurosci. Lett 1994;177:63–65. [PubMed: 7824184]
18. Wass CT, Lanier WL. Glucose modulation of ischemic brain injury: review and clinical recommendations. Mayo Clin. Proc 1996;71:801–812. [PubMed: 8691903]
19. Doerfler A, Schwab S, Hoffmann TT, Engelhorn T, Forsting M. Combination of decompressive craniectomy and mild hypothermia ameliorates infarction volume after permanent focal ischemia in rats. Stroke 2001;32:2675–2681. [PubMed: 11692033]
20. Lindauer U, Vogt J, Schuh-Hofer S, Dreier JP, Dirnagl U. Cerebrovascular vasodilation to extraluminal acidosis occurs via combined activation of ATP-sensitive and Ca2+-activated potassium channels. J. Cereb. Blood Flow Metab 2003;23:1227–1238. [PubMed: 14526233]
21. Tomiyama Y, Brian JE Jr. Todd MM. Cerebral blood flow during hemodilution and hypoxia in rats: role of ATP-sensitive potassium channels. Stroke 1999;30:1942–1947. [PubMed: 10471448]
22. Schwanstecher M, Loser S, Chudziak F, Bachmann C, Panten U. Photoaffinity labeling of the cerebral sulfonylurea receptor using a novel radioiodinated azidoglibenclamide analogue. J. Neurochem 1994;63:698–708. [PubMed: 8035194]
23. Dorschner H, Brekardin E, Uhde I, Schwanstecher C, Schwanstecher M. Stoichiometry of sulfonylurea-induced ATP-sensitive potassium channel closure. Mol. Pharmacol 1999;55:1060–1066. [PubMed: 10347249]
24. Xu Q, Ji YS, Schmedtje JF Jr. Sp1 increases expression of cyclooxygenase-2 in hypoxic vascular endothelium. Implications for the mechanisms of aortic aneurysm and heart failure. J. Biol. Chem 2000;275:24583–24589. [PubMed: 10825178]
25. Kaluz S, Kaluzova M, Stanbridge EJ. Expression of the hypoxia marker carbonic anhydrase IX is critically dependent on SP1 activity. Identification of a novel type of hypoxia-responsive enhancer. Cancer Res 2003;63:917–922. [PubMed: 12615703]
26. Young, W.; Constantini, S. The Neurobiology of Central Nervous System Trauma. Salzman, SK.; Faden, AI., editors. Oxford University Press; New York: 1994.
27. Wang Y, et al. Brain tissue sodium is a ticking clock telling time after arterial occlusion in rat focal cerebral ischemia. Stroke 2000;31:1386–1391. [PubMed: 10835461]
28. Toomey JR, et al. Inhibition of factor IX(a) is protective in a rat model of thromboembolic stroke. Stroke 2002;33:578–585. [PubMed: 11823673]
29. Nakabayashi K, et al. Evaluation of particulate embolic materials with MR imaging, scanning electron microscopy, and phase-contrast microscopy. AJNR Am. J. Neuroradiol 1997;18:485–491. [PubMed: 9090408]
30. Kawamura S, Yasui N, Shirasawa M, Fukasawa H. Rat middle cerebral artery occlusion using an intraluminal thread technique. Acta Neurochir. (Wien) 1991;109:126–132. [PubMed: 1858530]

31. Hua Y, Keep RF, Hoff JT, Xi G. Thrombin preconditioning attenuates brain edema induced by erythrocytes and iron. J. Cereb. Blood Flow Metab 2003;23:1448–1454. [PubMed: 14663340]

32. Gerzanich V, et al. Alternative splicing of cGMP-dependent protein kinase I in angiotensin-hypertension: novel mechanism for nitrate tolerance in vascular smooth muscle. Circ. Res 2003;93:805–812. [PubMed: 14512447]

33. Perillan PR, Chen M, Potts EA, Simard JM. Transforming growth factor-beta 1 regulates Kir2.3 inward rectifier K+ channels via phospholipase C and protein kinase C-delta in reactive astrocytes from adult rat brain. J. Biol. Chem 2002;277:1974–1980. [PubMed: 11713246]

34. Anisimov SV, Tarasov KV, Riordon D, Wobus AM, Boheler KR. SAGE identification of differentiation responsive genes in P19 embryonic cells induced to form cardiomyocytes in vitro. Mech. Dev 2002;117:25–74. [PubMed: 12204248]

35. Tsankova NM, Kumar A, Nestler EJ. Histone modifications at gene promoter regions in rat hippocampus after acute and chronic electroconvulsive seizures. J. Neurosci 2004;24:5603–5610. [PubMed: 15201333]

36. Hainsworth AH, Spadoni F, Lavaroni F, Bernardi G, Stefani A. Effects of extracellular pH on the interaction of sipatrigine and lamotrigine with high-voltage-activated (HVA) calcium channels in dissociated neurones of rat cortex. Neuropharmacology 2001;40:784–791. [PubMed: 11369032]

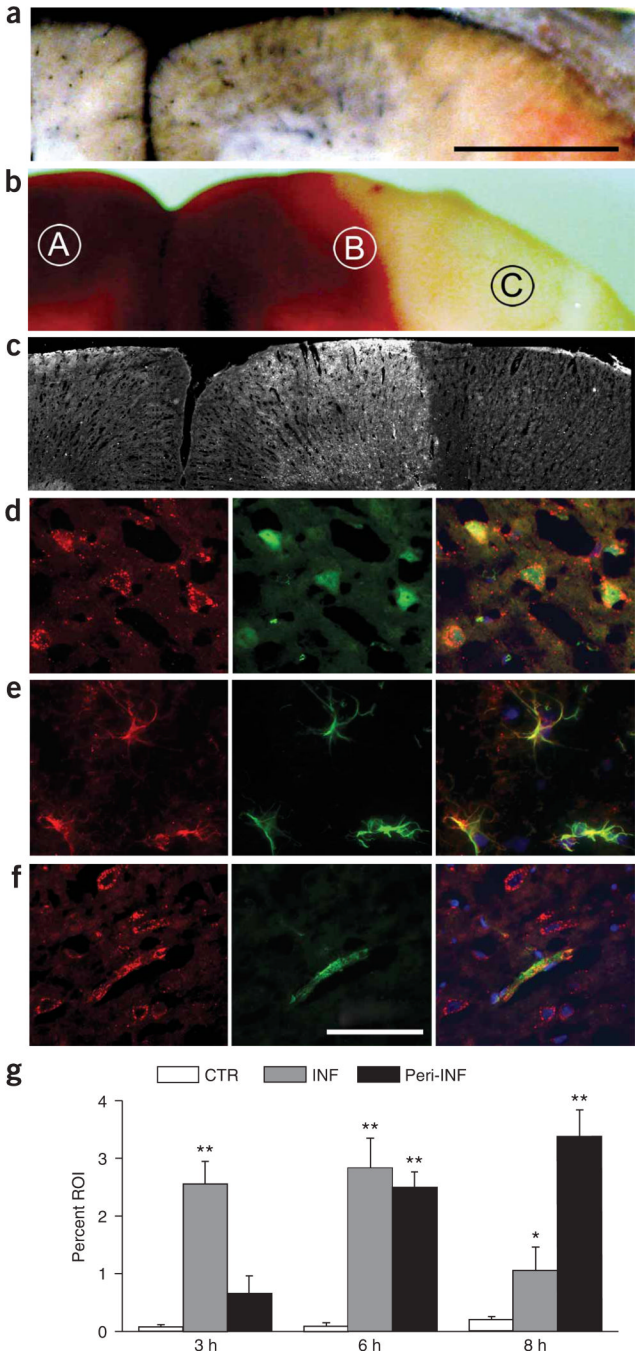

Figure 1.

SUR1 is upregulated in MCA stroke model. (**a–c**) Watershed area between MCA-anterior cerebral artery in three rats after MCAO, identified by postmortem perfusion of Evans blue dye and India ink (**a**), by TTC staining (**b**) and by immunofluorescence imaging for SUR1 at 8 h (**c**). Scale bar in **a**, 1 mm. (**d–f**) Immunofluorescence images showing SUR1 (red) in cells double labeled (green) for the neuronal marker NeuN (**d**), the astrocytic marker GFAP (**e**) or the endothelial cell marker von Willebrand factor (**f**). Scale bar in **f**, 50 μm. Superimposed images of double-labeled fields are also shown; image obtained either at 3 h from the core of the infarct (**d**) or at 8 h from the peri-infarct region (**e,f**). Cy3-conjugated (red) and FITC-conjugated (green) secondary antibodies were used. (**g**) Analysis of immunohistochemical

labeling for SUR1 in tissue sections obtained 3 h, 6 h and 8 h after MCAO; for all sections, labeling was analyzed in three regions, the uninvolved hemisphere, the peri-infarct region and the core of the infarct (labeled A, B and C, respectively, in **b**). CTR, control; INF, infarct region; Peri-INF, peri-infarct region. Data are expressed as the percent of the region of interest (ROI) showing specific labeling. Values are mean ± s.e.m.; three rats per time point. The following values were significantly different (by ANOVA): at 3 h, infarct versus control (**$P < 0.01$); at 6 h, infarct and peri-infarct versus control (**$P < 0.01$); at 8 h, infarct versus control (*$P < 0.05$) and peri-infarct versus control (**$P < 0.01$).

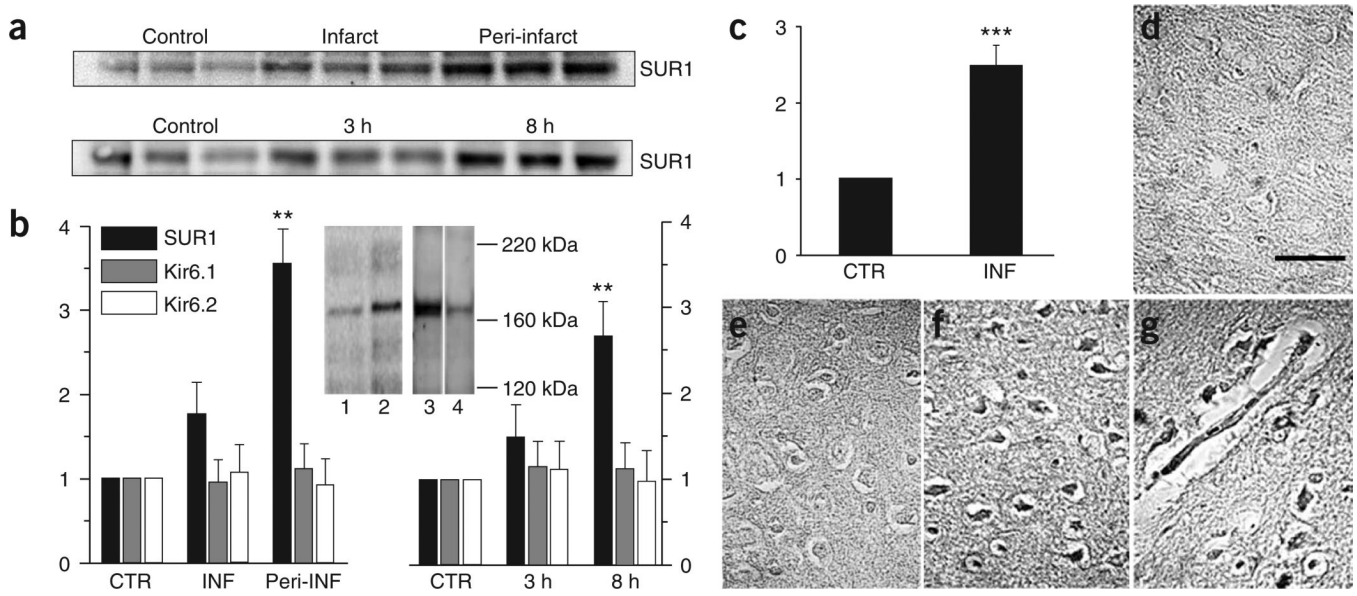

Figure 2.

SUR1 but not Kir6.1 or Kir6.2 is transcriptionally upregulated in MCA stroke model. (**a**) Immunoblots for SUR1 (180 kDa) at different locations (upper) and times (lower) after MCAO. Lysates were obtained at 8 h after MCAO from regions indicated (upper) or from TTC^+ peri-infarct regions at times indicated (lower). Each lane is from one rat. (**b**) Quantification of the data from **a** combined with comparable immunoblot data for Kir6.1 and Kir6.2. For each blot, data were normalized to values of β-actin and to the control data for that blot. $^{**}P < 0.01$. Peri-INF, peri-infarct region. Specificity of SUR1-specific antibody was confirmed by: (i) showing labeling of one band (180 kDa) in the range between 116−290 kDa in control and peri-infarct tissues at 8 h (insert, lanes 1 and 2, respectively); (ii) labeling of one band at the same mass was markedly reduced by *in vivo* knockdown of SUR1 expression in ischemic gliotic tissue using *in situ* infusion of antisense, but not random sequence, oligodeoxynucleotide (insert, lane 3 versus 4). (**c**) Quantification of real-time PCR for SUR1 in the core of the infarct (INF) and contralateral unaffected region (CTR) for three rats 3 h after MCAO. Data were normalized to values for Histone 1. $^{***}P < 0.001$. (**d–g**) *In situ* hybridization for SUR1, 3 h after MCAO. Paraffin sections showed that large neuron-like cells (**f**) and capillaries (**g**) in the core of the infarct were labeled with antisense probe, whereas tissues from the same areas on the control side were not (**d**). Scale bar in **d**, 50 μm. Core tissue labeled with 'sense' probe as a control is also shown (**e**). Pericellular edema is shown in **e–g**.

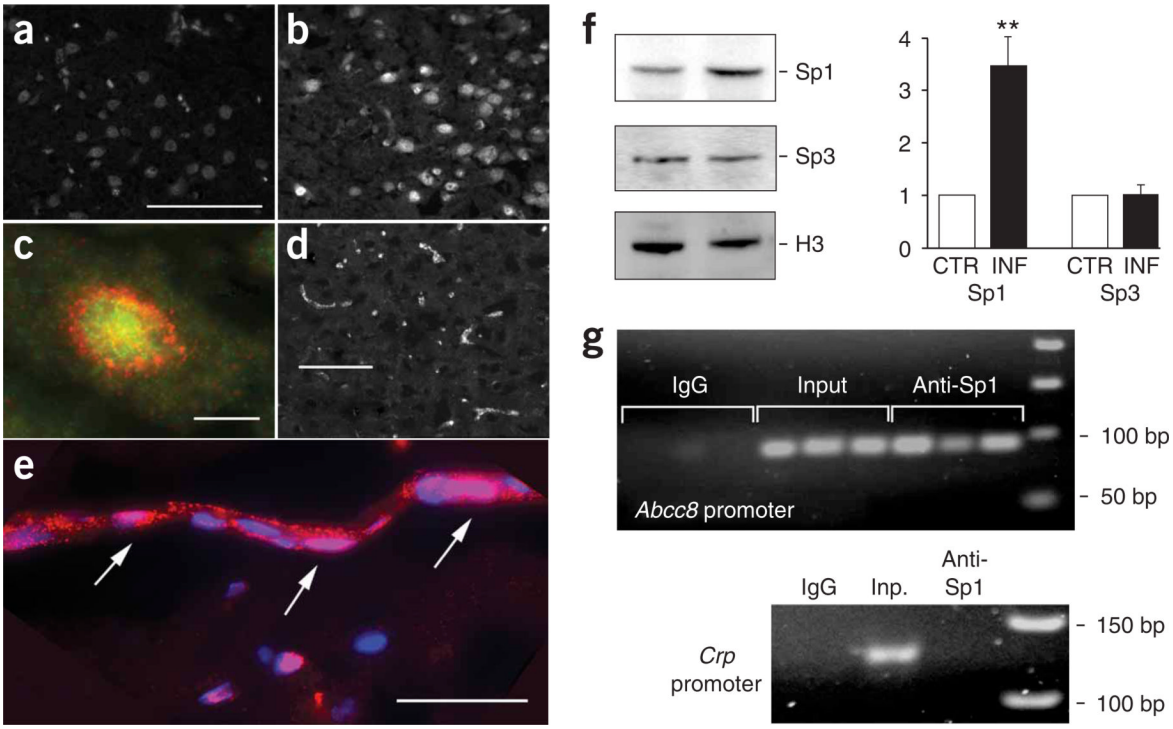

Figure 3.

Association of Sp1 and SUR1 promoter region in cerebral ischemia. (**a–e**) Immunofluorescence imaging for Sp1 in contralateral control region (**a**), in the core of the infarct 3 h after MCAO (**b,c**) and in the peri-infarct region 6 h after MCAO (**d,e**). In **c**, the section was double labeled for Sp1 (green) and SUR1 (red). In **e**, the section was also stained with the nuclear marker DAPI, with pink indicating nuclear localization of Sp1 (arrows). (**f**) Immunoblots of nuclear lysates and densitometric analyses of blots for Sp1 and Sp3, with Histone 3 (H3) as control, for contralateral control (CTR) and core (INF) tissues 3 h after MCAO. $^{**}P < 0.01$. (**g**) Electrophoretic gels of PCR products for the proximal promoter regions of *Abcc8* and the negative control, *Crp*. Chromatin isolated from the core of the infarct 2 h after MCAO in three different animals. DNA templates were: (i) 20 μg chromatin 'immunopreciptated' using nonspecific mouse IgG as negative control (IgG); (ii) 2 μg total chromatin as positive control (Input or Inp.); or (iii) 20 μg chromatin immunopreciptated using Sp1-specific antibody (Anti-Sp1). Scale bars in **a** and **d**, 100 μm; in **c**, 10 μm; in **e**, 25 μm.

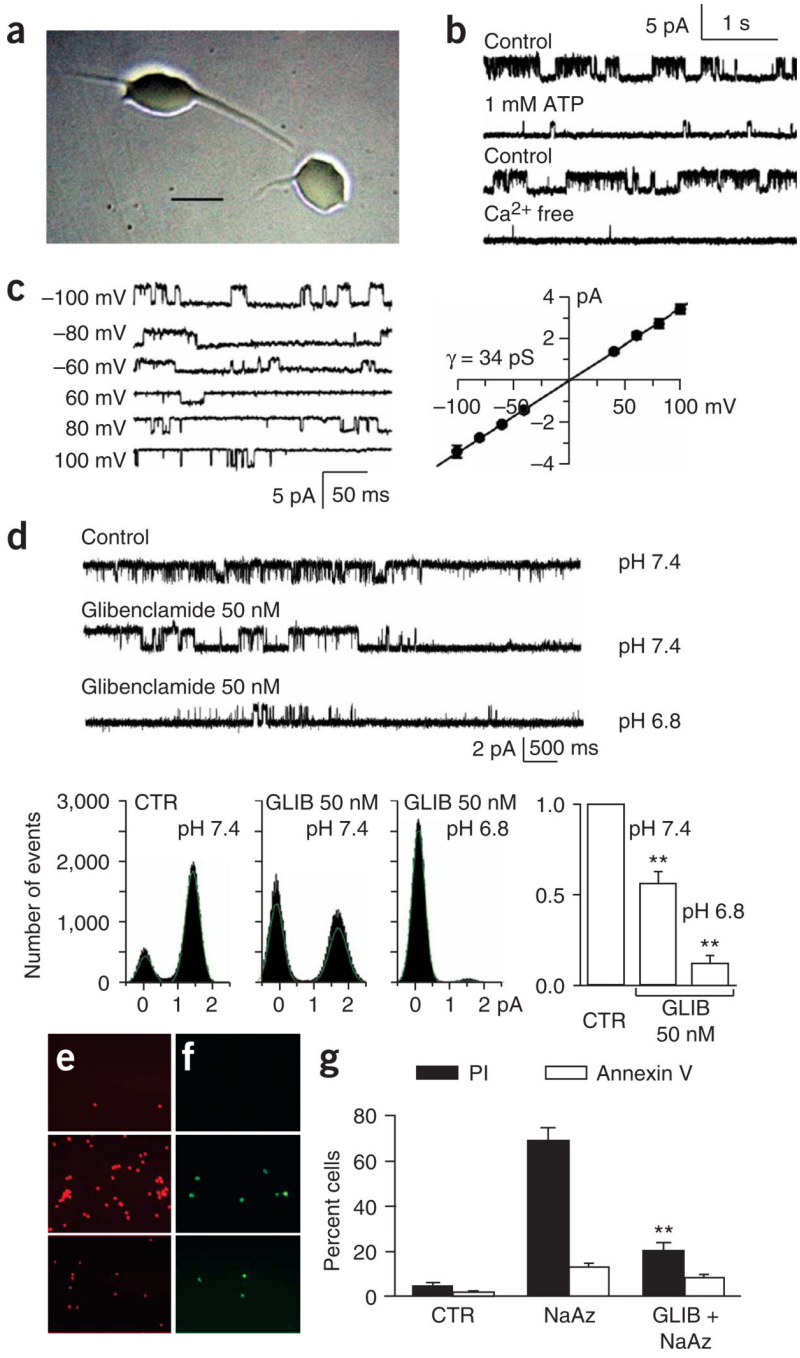

Figure 4.

Expression of functional $NC_{Ca\text{-}ATP}$ channels in cerebral ischemia. (**a**) Phase-contrast micrograph of neuron-like cells isolated from the core 3 h after MCAO. Scale bar, 20 μm. (**b**) Single-channel records of an inside-out patch from a neuron isolated from the core 3 h after MCAO, showing channel activity recorded under control conditions (Cs^+ as the charge carrier; 0 ATP, 1 μM Ca^{2+}, pH 7.4) before (first trace) and after addition of ATP (1 mM; second trace); records from another patch recorded under control conditions before (third trace) and after washout of Ca^{2+} (fourth trace); all records obtained at +100 mV. (**c**) Single-channel records of an inside-out patch from a neuron isolated from the core 3 h after MCAO, showing channel activity recorded at the potentials indicated, using K^+ as the charge carrier, with 0 ATP and 1

μM Ca^{2+} in the bath solution; open-channel slope conductance, 34 pS. Values are mean ± s.e.m. from three cells. (**d**) Single-channel records of an inside-out patch from a neuron isolated from the core 3 h after MCAO, showing channel activity recorded under control conditions (CTR; as above) before (first trace) and after addition of 50 nM glibenclamide (GLIB) at pH 7.4 (second trace), and after change to 50 nM glibenclamide at pH 6.8 (third trace). Open-time histograms for the same patch are shown. Bar graph shows mean change in open probability in three patches with 50 nM glibenclamide at pH 7.4 and pH 6.8. $^{**}P < 0.01$. (**e,f**) Fluorescence images showing propidium iodide (PI; red) and annexin V (green) labeling of astrocytes from ischemic gliotic tissue, 10 min after exposure to vehicle (upper panels), 10 min after exposure to 1 mM sodium azide (middle panels), and 10 min after exposure to 1 mM sodium azide after a 5-min pretreatment with 1 μM glibenclamide (lower panels). (**g**) Percent of cells labeled with PI (filled bars) and annexin V (open bars) for the same conditions as in **e,f**. NaAz, sodium azide. $^{**}P < 0.01$.

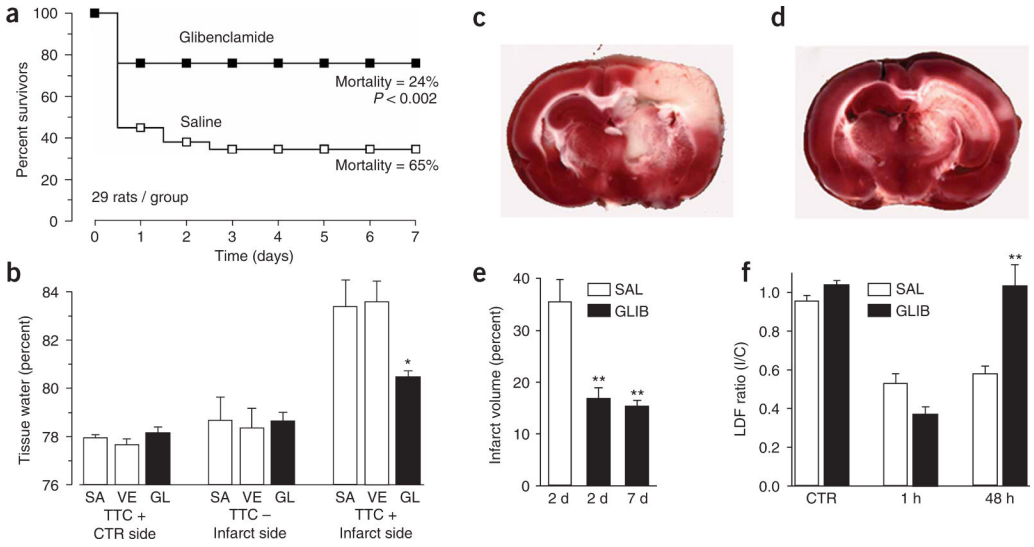

Figure 5.

Glibenclamide reduces mortality, edema and infarct volume, and improves cerebral blood flow in MCA stroke models. (**a**) Mortality was assessed during 7 d after MCAO (MCE model) in two treatment groups, each consisting of 19 female and 10 male rats, treated with either saline (open symbols) or glibenclamide (filled symbols). Mortality at 7 d was significantly different (by χ^2, $P < 0.002$); subgroup analyses for gender showed similar results. (**b**) Edema was assessed 8 h after MCAO (MCE model) in three treatment groups, each consisting of six male rats treated with either saline alone (SA), vehicle (VE; saline plus DMSO) or glibenclamide in vehicle (GL). Tissues were separated into TTC^+ and TTC^- portions before determining wet/dry weights. $^*P < 0.05$. (**c–e**) Infarct volume was assessed at 2 d or 7 d after MCAO (thromboembolic model) in three groups, consisting of 9, 9 and 7 male rats respectively, treated with either saline (SAL; 2 d) or glibenclamide (GLIB; 2 and 7 d). $^{**}P < 0.01$. Images of TTC-stained coronal sections 2 d after MCAO (thromboembolic model) in a rat treated with saline (**c**) and another treated with glibenclamide (**d**), showing cortical sparing with glibenclamide. (**f**) Relative cerebral blood flow, measured by laser Doppler flowmetry (LDF), before (CTR), 1 h after and 48 h after MCAO, in two groups, each consisting of four male rats, treated with either saline (open bars) or glibenclamide (filled bars). $^{**}P < 0.01$. I/C, ipsilateral/contralateral.

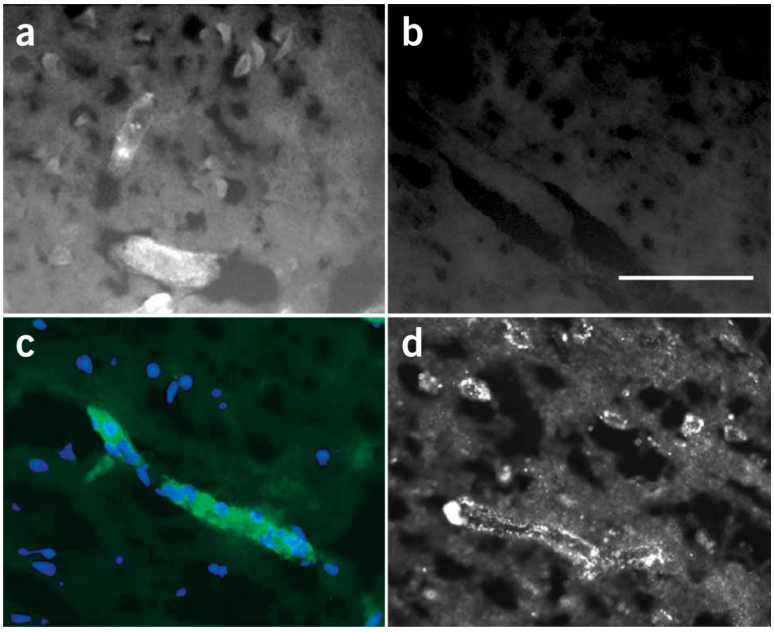

Figure 6.

Tissue distribution of BODIPY-glibenclamide in MCA stroke model. (**a–c**) Fluorescence images of brain sections in a rat 8 h after MCAO (MCE model) and administration of BODIPY-glibenclamide. Fluorescent labeling was evident in cells, microvessels (**a**) and capillaries (**c**) from ischemic regions, but not in the contralateral hemisphere (**b**). Scale bar in **b**, 100 μm. Images in **a,b** are from the same rat, taken with the same exposure time. In **c**, the single layer of nuclei labeled with DAPI (blue) confirms that the structure brightly labeled by BODIPY-glibenclamide (green) is a capillary. (**d**) Immunofluorescence image of a brain section from a rat 8 h after MCAO (MCE model) labeled with SUR1-specific antibody showing strong labeling in a capillary and in adjacent neuron-like cells.